Chapter 5

Understanding the dynamo in rapidly rotating stars

Having examined the flows in stellar activity cycles, it is evident that rapidly rotating stars behave differently from slowly rotating stars. Observations suggest that starspots appear near the polar regions in rapidly rotating stars. This is due to the stronger effect of the Coriolis force, which results in the parallel rise of the flux tubes while transporting from the deeper convection zone to the surface and thus appearing in the higher latitudes. In our previous studies, we overlooked this behavior; however, the Babcock-Leighton dynamo relies on generating a poloidal field through the decay and dispersals of tilted bipolar magnetic regions (BMRs). It is a promising paradigm for explaining the features of the solar magnetic cycle. In rapidly rotating stars, BMRs are expected to emerge at high latitudes, which are less efficient in generating the poloidal field due to poor cross-equatorial cancellation. Therefore, while modeling the same, it may raise one important question of whether the Babcock–Leighton dynamo process operates under these conditions or not. Hence, I shall be using a 3D kinematic dynamo model, STABLE, to explore this question. By taking large-scale flows from mean-field hydrodynamics models for stars rotating at different speeds, we conduct a series of dynamo simulations by considering the various cases.

5.1 Introduction

Low main sequence stars exhibit magnetic cycles analogous to the 11-year solar cycle (Baliunas et al., 1995). These cycles are characterized by the periodic variation in the star's magnetic field, manifested through e.g., changes in starspot number, chromospheric activity, and coronal emissions. The properties of these cycles, such as duration, amplitude, and overall activity, vary significantly among different stars. These variations are influenced by factors such as the star's age, rotation rate, surface temperature, internal structure, etc. In general, the more rapidly a star rotates, the more active it gets (Skumanich, 1972; Rengarajan, 1984). Noyes et al. (1984a) and Wright & Drake (2016) gave the activity-rotation relation using Ca II H & K and X-ray emissions, respectively. They demonstrated that activity increases with the rotation rate for slow rotators but tends to saturate for fast-rotating stars. There are a few pieces of evidence that suggest the activity may even decline somewhat in the most rapid rotators (e.g., James et al., 2000). A similar resemblance is also observed between rotation rate and estimates of the unsigned surface magnetic flux (Saar, 2001; Reiners & Basri, 2009). A complete theoretical understanding of the rotation-activity relationship is still unclear (Işık et al., 2023). These phenomena likely depend on factors like magnetic flux emergence, chromospheric and coronal heating, and mass loss mechanisms. However, it is widely believed that the basic rotation-activity relationship is due to an inherent connection between rotation and the dynamo process (Noyes et al., 1984a; Baliunas et al., 1995).

A large-scale dynamo, driven by the helical convection and differential rotation, is fundamental to generating and sustaining the magnetic fields in the Sun (Parker, 1955b). As the sun-like stars have convection zones (CZs) in their outer layers like the Sun, it is natural to expect that these stars also support dynamo action through which the stellar magnetic cycles are maintained. Some of the stars (e.g., HD 10476, HD 16160, etc.) have cycles similar to the solar cycle, which suggests that a similar dynamo that is operating in our Sun might be working in other sun-like stars (also see Garg et al., 2019; Jeffers et al., 2022). In this dynamo process, shearing due to differential rotation produces a toroidal magnetic

field from a poloidal one (the Ω effect), while cyclonic convection (the α effect) regenerates the poloidal magnetic field. Although the α effect, which involves the lifting and twisting of the toroidal field due to helical convection, is a potential way to generate the poloidal field, the Babcock-Leighton (BL) process has strong observational support and is now considered the main method for generating the poloidal field in the Sun (Dasi-Espuig et al., 2010; Kitchatinov & Olemskoy, 2011b; Priyal et al., 2014; Cameron & Schüssler, 2015).

In this process, tilted sunspot groups (more accurately, the bipolar magnetic regions) decay and disperse to produce a poloidal field through turbulent diffusion, meridional flow, and differential rotation.

The key ingredients in the Babcock–Leighton process are the tilt and the latitudinal position of BMR emergence. In fact, surface flux transport (SFT) simulations (Cameron & Schüssler, 2015; Jiang et al., 2014b) dynamo models (Karak & Miesch, 2018; Kumar et al., 2024a), and analytic calculations (Petrovay et al., 2020) show that the higher the latitude, the less effective the poloidal field generation is (Muñoz-Jaramillo et al., 2013; Cameron & Schüssler, 2015; Jiang et al., 2014b). This phenomenon is a key to well-known latitudinal quenching (Petrovay, 2020; Jiang, 2020; Karak, 2020), implying that stronger cycles which produce sunspots at higher latitudes are less effective in generating a poloidal field. In short, latitude plays a crucial role in the effectiveness of the BL process.

Since starspots are also expected to show similar features as of sunspots, we expect BL process to operate in other stars. Previous studies already employed axisymmetric kinematic dynamo model by parameterizing BL process with a non-local α effect to explain features of stellar cycles (Nandy & Martens, 2007; Jouve et al., 2010; Karak et al., 2014b; Hazra et al., 2019a; Vashishth et al., 2023). In these previous stellar dynamo models, the Babcock–Leighton process is not adequately captured; it is through a non-local α term, which is included as a poloidal field source term. As starspots are believed to be produced through the rise of the toroidal flux tubes from the deeper CZ and during the rise of flux tubes, the Coriolis force acting on the diverging flows arising from the apex of

the tubes, the tilt and the emerging latitudes are expected to increase with the increase of rotation rates of stars (Işık et al., 2018). Most stars are born with rapid rotation and in their early stages, the flows in their CZs experience more Coriolis force, leading to larger tilt angles and spots appearing at high latitudes. Observations also suggest that in young-rapidly rotating sun-like stars, spots appear at high latitudes (Schuessler & Solanki, 1992a; Schuessler et al., 1996; Luo et al., 2022). This naturally raises a question: does the BL process operate in rapidly rotating stars?

In the present study, we employ a 3D kinematic solar dynamo model STABLE (Surface flux Transport And Babcock–LEighton; Miesch & Dikpati, 2014; Miesch & Teweldebirhan, 2016; Karak & Miesch, 2017) to explore the functioning of the Babcock–Leighton process in the stars with rotation rates varying from 1 day to 30 days. In this work, we incorporate meridional flow and differential rotation from a mean-field hydrodynamics model (Kitchatinov & Olemskoy, 2011a) for stars of different rotation periods and depths of CZ. Our results will have an implication for stars, particularly young-fast rotators whose cycles vary with strengths and durations (e.g., Baliunas et al., 1995; Garg et al., 2019). Thus, our study aims to identify how the Babcock–Leighton process operates across a range of stars, from rapid to slow rotators, and how cycle strength and duration vary with rotation rate. In section 4.2, we present our model, while in section 5.3 we discuss our results. Finally, in section 5.4, we summarize our results and highlight the conclusion.

5.2 Application of STABLE to stars

The STABLE dynamo model was original designed to reproduce the magnetic field of Sun by utilizing the large-scale flows and the deposition and decay of BMRs on the solar surface (Babcock–Leighton process) guided by solar observations. This model produces many basic features of the solar cycle, including its long-term variation (Karak & Miesch, 2017, 2018; Karak, 2020). However, when we apply this model we need to make some essential modification to it. The obvious modification will be in the large-scale flow.

We take the profiles of the meridional circulation and the differential rotation from the

mean-field hydrodynamics models of Kitchatinov & Olemskoy (2011a) for stars of rotation periods of 1, 3, 7, 10, 15, 20, 25.38 (solar value), and 30 days. Kitchatinov & Olemskoy (2011a) model produces solar-like differential rotations for all these stars by solving the steady state equation of motion and the entropy equation in combination of EZ stellar evolution code (Paxton, 2004) to specify the structure of a $1M_0$ mass star as a function of age and the gyrochronology relation to identify the rotation rate for the star of a given age (Barnes et al., 2005). Let me now discuss the numerical model in details. Firstly, the model solves the the steady state motion equation in the following form,

$$(\boldsymbol{V}.\nabla)\,\boldsymbol{V} + \frac{1}{\boldsymbol{\rho}}\nabla\boldsymbol{P} - g = \frac{1}{\boldsymbol{\rho}}\nabla.\boldsymbol{R}, \tag{5.1}$$

where $\boldsymbol{R}$ represents the Reynolds stresses, $R_{ij} = \rho Q_{ij}$, through which the convective velocities v_i contribute to the steady-state equation. Here, $Q_{ij} = \langle v_i v_j \rangle$ is the correlation tensor of the fluctuating velocities. The differential rotation arises due to angular momentum transport facilitated by convection and meridional flow, and the convective transport of angular momentum is governed by the correlations, $Q_{\phi r}$ and $Q_{\phi\theta}$, of azimuthal and meridional velocities. The correlations, Q_{ij}, consist of the eddy viscosities (Q^{ν}_{ij}) as well as the non-viscous part (Q^{Λ}_{ij}) (Λ-effect), and each of them is represented as,

$$Q_{ij} = Q^{\nu}_{ij} + Q^{\Lambda}_{ij},$$

$$Q^{\nu}_{ij} = -N_{ijkl}\frac{\partial V_k}{\partial r_l}, \tag{5.2}$$

$$Q_{r\phi}{}^{\Lambda} = \frac{\tau l^4 g}{15 H_\rho c_{\rm p}}\frac{\partial S}{\partial r}\Omega\sin\theta\left(V(\Omega^*) + H(\Omega^*)\cos^2\theta\right), \tag{5.3}$$

$$Q_{\theta\phi}{}^{\Lambda} = -\frac{\tau l^4 g}{15 H_\rho c_{\rm p}}\frac{\partial S}{\partial r}\Omega\sin^2\theta\cos^2\theta, H(\Omega^*). \tag{5.4}$$

Here, N is the eddy transport coefficients, τ is the correlation time of convective turbulence, l is the correlation length, H_ρ is the density scale height, $c_{\rm p}$ is the specific heat capacity at constant pressure, S is the specific entropy, and V and H are the dimensionless functions of the Coriolis number $\Omega^* = 2\tau\Omega$. The turbulence intensity and the eddy trans-

port coefficients can be expressed in terms of the entropy gradients and are solved together with the equation of motion. The Λ coefficients are described based on the quasi-linear theory of turbulent transport (Rüdiger et al., 2013). Now the eddy thermal diffusivity has a turnable parameter, C_ϕ,

$$X_{ij} = -\frac{\tau l^2 g}{12 c_p} \frac{\partial S}{\partial r} \left(\phi(\Omega^*) \delta_{ij} + C_\phi(\Omega^*) \hat{\Omega}_i \hat{\Omega}_j \right). \tag{5.5}$$

The diffusivity is anisotropic and this anisotropy is induced by rotation. When rotation is slow ($\Omega^* \rightarrow 0$), the second term within the equation disappears ($\phi(0) = 0$), leading to isotropic diffusivity. However, the presence of finite anisotropy in a rotating star plays a crucial role in its differential rotation structure, causing a subtle increase in average temperature at higher latitudes. This temperature gradient is crucial for deviations from the Taylor–Proudman theorem, which typically predicts cylinder-shaped rotation (Rüdiger et al., 2013). The use of $C_\chi = 1.5$ in the model aligns well with findings from helioseismology; hence, this value was kept constant in stellar simulations. To model the differential rotation, it's necessary to define the star's structure. The EZ stellar evolution code by Paxton (2004) is employed to outline the structure of a $1M$ star over time. Additionally, Barnes (2007)'s gyrochronology relation is used to determine the rotational speed for stars at various ages, facilitating a series of models that illustrate differential rotation and meridional flow in the Sun through different stages. This modeling approach is detailed in Kitchatinov & Olemskoy (2011a) and Kitchatinov & Olemskoy (2012a), showing that the solar-type rotation typically features a faster-rotating equator than the poles. Conversely, only under conditions of very slow rotation $e.g.$, $P_{\rm rot} = 60$ days and significantly reduced anisotropy in heat transport does anti-solar rotation appear, a finding supported by both Kitchatinov & Olemskoy (2012a) and further studies by Gastine et al. (2014) and Karak et al. (2014a).

Hence, this numerical model jointly solves the mean-field equations for the angular velocity, meridional flow, and heat transport in a spherical layer of a stellar convection zone. The model produces the solar-type differential rotation as a consequence of angular mo-

mentum fluxes. The one-cell per hemisphere meridional flow predicted by the model for the sun agrees with the recent seismological detection (Rajaguru & Antia, 2015; Gizon et al., 2020). Also, the computed dependence of differential rotation on stellar rotation rate and spectral type (Kitchatinov & Olemskoy, 2012c) is in at least qualitative agreement with observations by Barnes et al. (2005) and Balona & Abedigamba (2016). The model, however, does not produce the tachocline self-consistently; rather, it has the lower boundary at $0.72R_s$ (R_s being the stellar radius). Therefore, the tachocline in our dynamo model is formed by smoothly varying the $\Omega_{\rm model}(r,\theta)$ from the differential rotation model at $r = 0.72R_s$ to the value of the rotation rate at the core $\Omega_{\rm core}$ in the following way:

$$\Omega(r,\theta) = \Omega_{\rm model}(r,\theta) + \frac{1}{2}\left[\Omega_{\rm core} - \Omega_{\rm model}(0.72R_s,\theta)\right] \times \left[1 - {\rm erf}\left(\frac{r - 0.7R_s}{0.02R_s}\right)\right]. \quad (5.6)$$

The profiles for the differential rotations are given in several prior publications, notably outlined in Karak et al. (2014b); Hazra et al. (2019a); Vashishth (2024a) and thus not reproduced again here. With the above flows, we conduct several stellar dynamo simulations to explore the operation of Babcock–Leighton process in solar-type stars. We consider following cases.

5.2.1 Case I

In this case, we do not make any changes in the STABLE model except the large-scale flow as mentioned above. We recall that in this model, the SpotMaker algorithm places a spot on the surface at the same latitude where it is linked to the azimuthal field at the base of CZ; that is, if θ_b is the latitude of the BMR where $\hat{B}$ (as computed from Eq. (4.6)) exceeds B_t in the CZ, then θ_s is the latitude where the spot is deposited on the surface, then we have taken, $\theta_b = \theta_s$. This scenario is referred to as Case I in this work, where the spot is positioned radially.

5.2.2 Case II

Observations show spots near the poles in rapidly rotating stars. The possible explanation for these polar spots is the stronger effect of the Coriolis force on the toroidal flux tube,

which causes the flux tubes to rise parallel to the rotation axis as they travel from the deeper CZ to the surface (Schuessler & Solanki, 1992a; Schuessler et al., 1996; Luo et al., 2022). Theory show that for a rotation period less than about 10 days, the toroidal flux tubes rise parallel to the rotation axis (Schuessler & Solanki, 1992a).

Therefore in this case, we capture this effect by placing the spots parallel to the axis of rotation for stars of rotation period shorter than 10 days. Accordingly, θ_s will be computed based on the value of θ_b to place the spot parallel to the rotation axis. This scenario whose everything else are the same as Case I is referred as Case II.

5.2.3 Case III

We move further by capturing the increase of the tilt angle with the rotation rate of stars. So far in Cases I-II, we were considering the amplitude of Joy's law the same for all stars and it was given by Eq. (4.9). However, theoretical studies using thin flux tube model simulations indicate that the tilt angle of BMR increases with the rotation rate (Işık et al., 2018). Hence, in this case, we make the tilt rotation dependent in addition to the parallel rise of the toroidal flux for stars with rotation period less than 10 days (Case II). Since the relationship between tilt and rotation rate is not well understood, we use the following form to capture this dependency:

$$\delta_0 = \delta_0 \left(\frac{P_s}{P_*} \right)^{\zeta}, \tag{5.7}$$

where P_* and P_s are the rotation period of the star and the sun, respectively, and ζ is the factor by which $\frac{P_*}{P_s}$ influences the tilt angle.

5.3 Results and Discussion

We have performed dynamo simulations for $1\ M_\odot$ stars with rotation periods ranging from 1 day to 30 days for different cases as discussed above. Since the primary objective of this work is to explore dynamo operation in rapidly rotating stars, we first present a detailed

analysis of the results for the star with a 1-day rotation period.

5.3.1 Star of 1 day rotation period

The star with a rotation period of 1 day produces regular polarity reversals approximately every 20 years in Case I, as shown in Fig. 5.1. The magnetic field is predominantly dipolar, with a strong toroidal field concentrated around 50° latitudes. In this case (radial spot deposition), spots are deposited at low latitudes, which maintain a dipolar magnetic field through the efficient cross-equatorial cancellation of the leading polarity flux from the other hemisphere (e.g., Durrant et al., 2004; Cameron et al., 2013; Karak & Miesch, 2018). The results drastically change in Case II, where spots are deposited at latitudes aligned parallel to the rotation axis as guided by the theory of magnetic flux rise in rapidly rotating stars (Schuessler et al., 1996; Granzer et al., 2000; Işık et al., 2011, 2018). As shown in Fig. 5.2, all BMRs in this case, appear above approximately 50° latitude, and these high-latitude spots are inefficient for the cross-equatorial cancellation. The leading polarity flux cannot cancel the opposite polarity one from the other hemisphere, resulting in a predominantly quadrupolar magnetic field.

In Case III, where the BMR tilt is scaled by the rotation rate of the star (Eq. (5.7)), we observe a strong increase in the magnetic field strength. The increase in field is due to the increase in the tilt angle of BMR. The magnetic field polarity is still remains quadrupolar (Fig. 5.3a) due to the high latitudes of spot emergence. Aditionally, the spot eruption rate is quite high in this case. This is because the time delay (between two successive spots) is regulated by the magnetic field—with the increase of toroidal field the delay distribution becomes narrow; see Eq. (4.8). However, the delay cannot become smaller than the numerical time step, and thus, the monthly number of spots cannot exceed a certain value during the magnetic maximum; see Fig. 5.3(b).

Furthermore, to check the robustness of the dependence of the rotation rate on the amplitude of Joy's law, we used a sample rotation period of 1 day and varied the parameter ζ in the range of 0 to 1. As shown in Fig. 5.4, we observe that the magnetic field strength

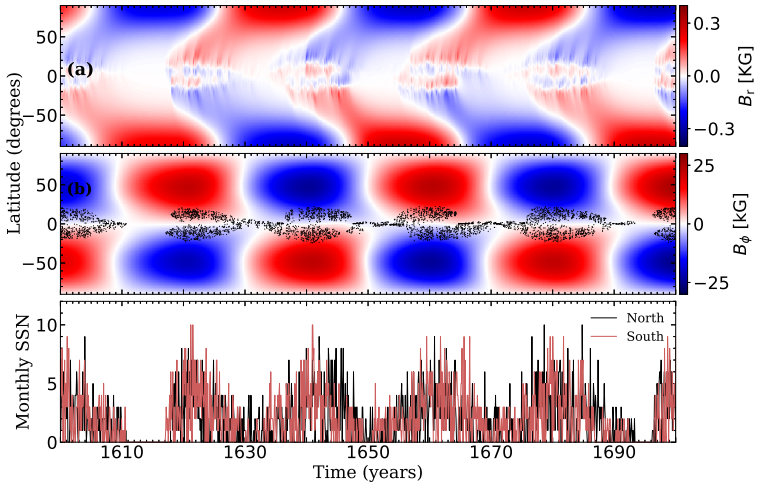

Figure 5.1: (a) Time-latitude distribution of the surface radial magnetic field $B_{\rm r}$ [in kG], and (b) toroidal field along with starspot distribution (black dots) for a star of 1 day rotation period for Case I.

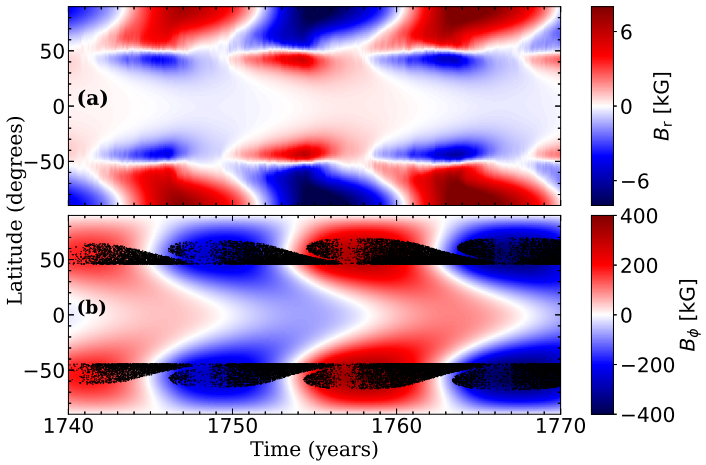

Figure 5.2: Same as Fig. 5.1, but for Case II.

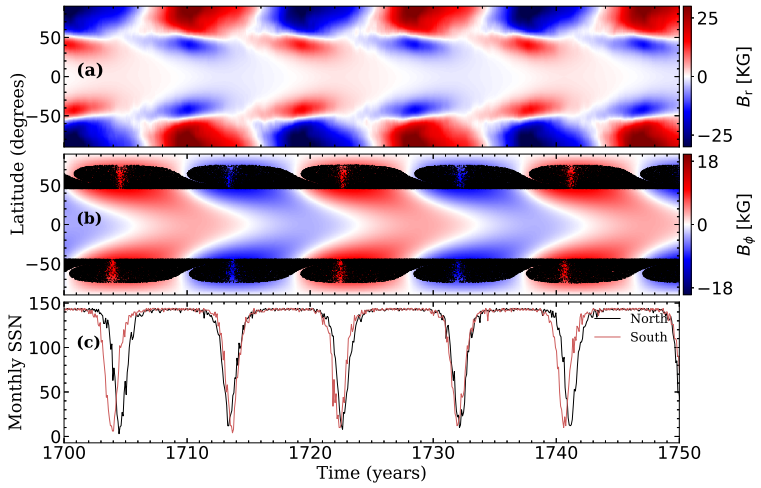

Figure 5.3: Same as Fig. 5.1, but for Case III.

increases with greater dependence of rotation period on Joy's law. Additionally, the cycle period becomes shorter with increasing dependency on rotation rate. This is because with the increase of ζ the value of the BMR tilt increases and the efficiency of poloidal field increases which makes the cycle period shorter.

5.3.2 Stars of different rotation periods

We now consider the results of stars at different rotation rates. In Case I for which spots are deposited in radial direction, i.e., low-latitude eruptions, we observe regular polarity reversals and smooth cycles with predominantly dipolar magnetic field for all the stars. As a representative example, the distribution of the surface radial field for the 10 day rotating star is shown in Fig. 5.5(a).

In both Cases II and III also, we observe magnetic cycle with regular polarity reversal. But again because of the avoidance of low-latitude spots (parallel rise), we again observe quadrupolar magnetic field for all stars with rotation period up to 10 days. A representative magnetic field distribution for the 10 day rotating star is shown in Fig. 5.5(b) and (c), respectively, for Cases II and III. Major difference between these two cases is that the magnetic field in Case III is strong as the tilt angle is scaled up by the rotation rate. With the increase of rotation period from 10 days to 15 days, as the spot eruption zone moves

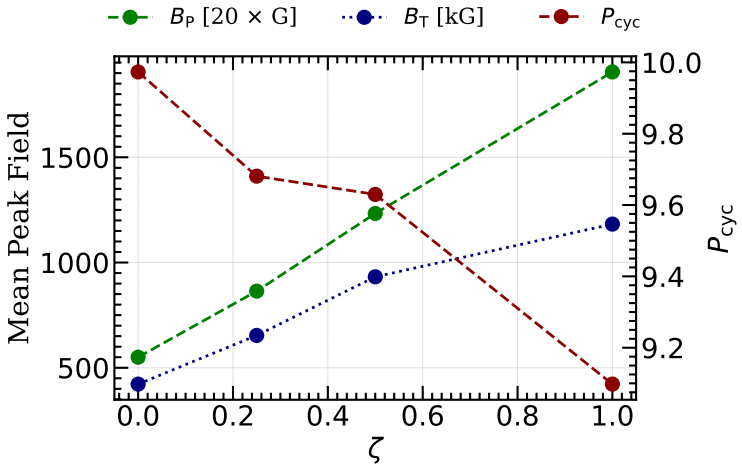

Figure 5.4: The variation of the mean peak field for a rotation period of 1 day with the ζ, the factor that shows the dependency of the rotation period on the tilt angle.

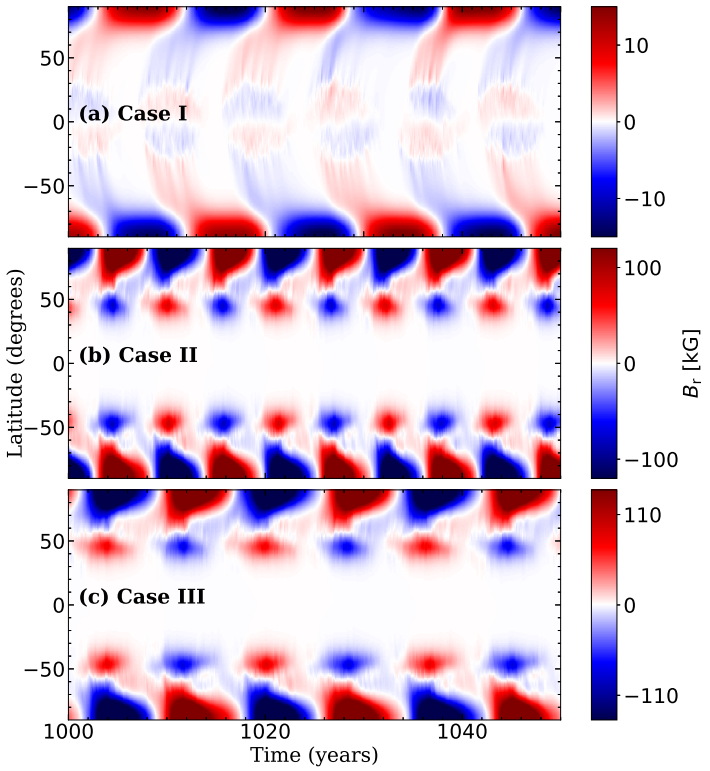

Figure 5.5: Time-latitude distribution of the surface radial magnetic field B_r [in kG] for a star of 10 days rotation period for Cases I–III.

to low latitude which causes to decrase the tilt, the magnetic field strength drops and it continues to drop till the lowest considered case of 30 days rotation period. Its field distributions for Cases I and III are shown in Fig. 5.6. Here we again recover regular solar-like oscillation with dipolar parity of magnetic field. Case I and III display almost similar solution because the only difference in Case III is that amplitude of Joy's law which is by a factor 25.38/30.

We note that the polarity of the magnetic field is independent of the initial magnetic configuration. In Case III (parallel rise) for fast rotators, we find that even if the simulations are initialized with dipolar parity, the magnetic field configuration flips to a quadrupolar one. Similarly, in Case I (radial rise/low latitude spots) even when we initialize the simulation with quadrupolar field, it flips to dipolar.

Interestingly, in previous axisymmetric dynamo simulations (Hazra et al., 2019b; Vashishth, 2022) with α parametrization for the Babcock–Leighton process for stars with rotation period less than 10 days also produced quadrupolar magnetic field. In our 3D dynamo model, in Case I we always get dipolar parity because of the low-latitude eruption.

The variation of the toroidal and poloidal magnetic field strengths as function of the rotation period is shown in Fig. 5.7. For Case I (red points), both fields slowly increase with the increase of rotation period up to about 10 days and decreases beyond that point. The trend is due to the fact that as a star rotates faster, the shear decreases, and the omega effect decreases as well (Kitchatinov & Rüdiger, 1999; Kitchatinov & Olemskoy, 2012b) (we confirmed this decreasing trend after computing $\Delta\Omega$ for each star). At this point, the meridional flow becomes a significant factor in determining the trend of the poloidal and toroidal fields with the rotation period, as recently demonstrated in Vashishth & Karak (2024a). For fast rotators, starting with a rotation period of 1 day, the surface meridional flow is very strong, while the flow within the bulk of the CZ is negligible (see Figure 7 of Vashishth & Karak, 2024a), both contributing to an extremely weak polar field (also see Figure 8a of Vashishth & Karak, 2024a). As the rotation period increases, the meridional flow within the bulk strengthens, leading to an increase in the polar field. Conversely, at

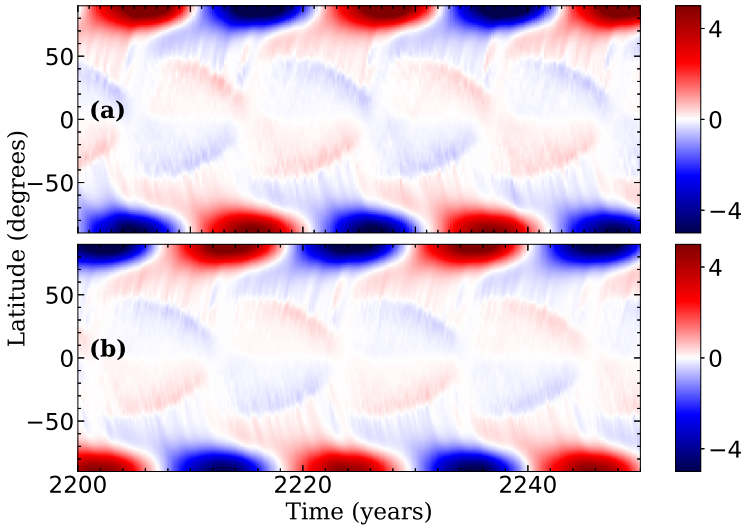

Figure 5.6: Time-latitude distribution of the surface radial magnetic field $B_{\rm r}$ [in kG] for a star of 30 days rotation period for Cases I & III (Note: For stars with rotation periods $\geq$ 15 days, Case III becomes identical to Case II).

a rotation period of 30 days, the bulk flow is strongest, but the surface flow is weakest, resulting in a weak polar field again. When the rotation period decreases from this point, the surface flow intensifies, contributing to a stronger polar field. Thus, the polar field increases when transitioning from low to high meridional flow in the bulk or from low to high surface flow.

The variations of the magnetic field strengths for cases II and III as a function of rotation period are shown by green and blue points in Fig. 5.7. For Case III, in all the stars, ζ in Eq. (5.7) is taken as 1. For Case II, where the BMRs rise parallel to the rotation axis in rapidly rotating stars, we observe a similar increasing trend in the poloidal field as in Case I, whereas the toroidal field decreases a bit at rotation period 3 days and increases thereafter. This decrease in the magnetic field with the rotation rate is again due to the reduction in the variation of angular velocity and the decrease in the meridional flow within the bulk of CZ with the increase in the rotation rate of the star.

We note that Case I and Case II become identical for stars of rotation period $\geq$ 15 days. Therefore, the behavior for Case II is interesting because the activity initially increases with the increase of rotation rate (from right to left in Fig. 5.7), and then it decreases. This

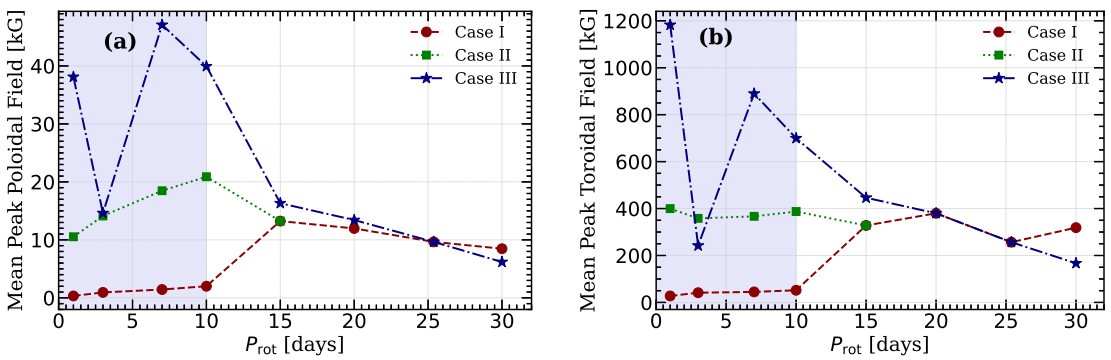

Figure 5.7: Variation of the mean peak (a) toroidal and (b) poloidal magnetic fields with the rotation period of the star for different cases of simulations. The shaded area represents the range of rotation periods for which the spots are deposited in parallel to the rotation axis, i.e., void of low-latitude eruptions.

behavior is somewhat consistent with the stellar observation of coronal and chromospheric emission vs rotation rate (Noyes et al., 1984a; Wright, 2016) and previous results from axisymmetric dynamos (Karak et al., 2014b; Hazra et al., 2019b; Vashishth et al., 2023). Case III shows somewhat similar behavior, except the activity level increases rapidly with the decrease of the rotation period. This is because, in this case, the tilt increases with the decrease of the rotation period. In the rapid rotator regime, the fields show a somewhat complex trend: they decrease after a rotation period of 1 day, then increase suddenly after a rotation period of 7 days, and decrease again. This decreasing trend remains consistent in the slow rotator regime.

5.3.3 Cycle period vs rotation period

We now analyze the cycle duration of stars for all cases, and the trends are shown in Fig. 5.8. In Case I, we observe a monotonic decrease in the cycle period with the rotation period for fast rotators. This happens because, as the rotation period decreases (or rotation rate increases), the meridional flow becomes weaker (although the flow speed increases in the thin layers near the top and bottom boundaries). However, after a rotation period of 15 days, there is a slight increase in the cycle period at higher rotation periods. The slight increase in the cycle period (after a rotation period of 15 days) is because the generation of the poloidal field weakens as the star spins down, and the poloidal field needs more time to

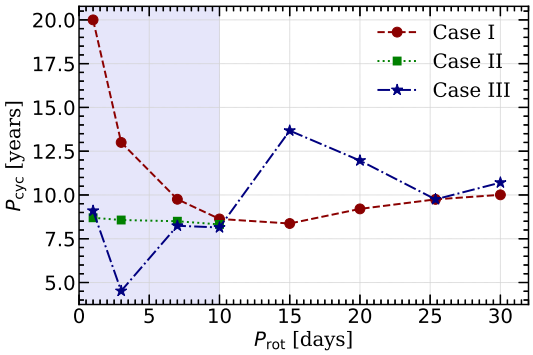

Figure 5.8: The variation of magnetic cycle period with the rotation period.

reverse the old field. This monotonic decrease in cycle duration for rapidly rotating stars is also observed in Case II. Limited observations (Boro Saikia et al., 2018) seem to show a rapid increase in the cycle period with the increase of the rotation rate for fast-rotating stars, which is consistent with the trend found in our Cases I–II. Meanwhile, the observed data for slow rotators show an increasing trend of activity cycle period with an increase in rotation period, which somewhat agrees with our Case I. However, for Case III, the trend is quite complicated, increasing first till the rotation period of 15 days and declining afterward.

5.4 Conclusions

In this study, we use the 3D STABLE (Surface flux Transport And Babcock–Leighton) dynamo model, which realistically captures the generation of poloidal field—the decay and dispersal of starspots to explore the operation of Babcock–Leighton dynamo in solar-type stars. In particular, we address the possibility of Babcock–Leighton dynamo in rapidly rotating stars of rotation period 1 day and more for which starspots are predominately formed at high latitudes.

In our study, we consider $1 M_{\odot}$ mass stars of different rotation periods starting from 1 day to 30 days. Meridional flow and differential rotation profiles are derived from a mean-field hydrodynamics model tailored for stars with different rotation periods. These profiles are incorporated into the dynamo model to investigate the operation of the Babcock–Leighton

dynamo under various scenarios.

Our findings show that the Babcock–Leighton dynamo efficiently operates with regular polarity reversals and predominantly dipolar parity across all stars considered, except for rapidly rotating stars with rotation periods ≤ 10 days. For these stars, when the toroidal flux rises parallel to the rotation axis, spots appear at high latitudes, leading to a low-latitude zone of avoidance. These high-latitude spots lead to inefficient cross-equatorial cancellation of the leading polarity flux across the equator, thereby maintaining a quadrupolar magnetic field, in contrast to the dipolar field as obtained in the radial rise scenario with low-latitude spots.

Additionally, we find consistent results of increasing magnetic field strength with the decrease of rotation period and a tendency of saturation (or even decrease) of magnetic field for stars with rotation period less than 10 days, in qualitative agreement with observations (Noyes et al., 1984a; Wright et al., 2011).

We are further exploring the dynamo operation by considering more realistic time delay distribution, bigger spots near polar regions, and allowing low latitude eruptions of highly supercritical fields (as recently emphasized by Işık et al., 2024) for stars having rapid rotation.